Journal of
Materials Chemistry C

Materials for optical, magnetic and electronic devices

Accepted Manuscript

This article can be cited before page numbers have been issued, to do this please use: D. Li, J. Zou, C. Wei, Y. Zhou, L. Wang, W. Zhang and G. Yu, *J. Mater. Chem. C*, 2019, DOI: 10.1039/C9TC03726H.

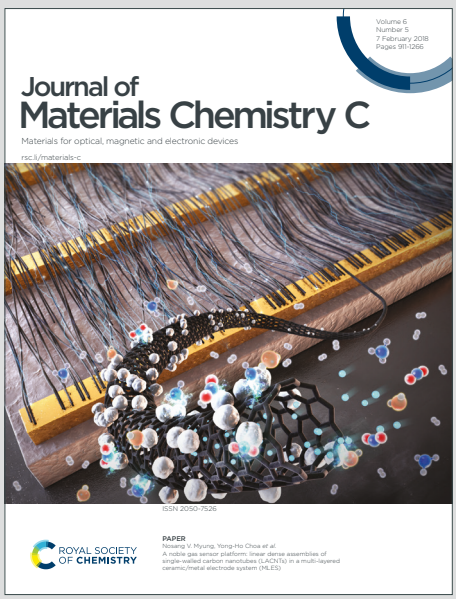

ROYAL SOCIETY OF CHEMISTRY

rsc.li/materials-c

View Article Online
DOI: 10.1039/C9TC03726H

ARTICLE

Small-molecule semiconductors containing dithienylacrylonitrile for high-performance organic field-effect transistors

Received 00th January 20xx,
Accepted 00th January 20xx

DOI: 10.1039/x0xx00000x

Dizao Li,[a] Jiabin Zou,[ab] Congyuan Wei,[ac] Yankai Zhou,[ab] Liping Wang,*[b] Weifeng Zhang[a] and Gui Yu*[ac]

We designed and synthesized four donor–acceptor-type conjugated small-molecule compounds DPP-CN-DTE-1, DPP-CN-DTE-2, DPP-DTE-CN-1 and DPP-DTE-CN-2. The four compounds contained long alkyl side chains on the diketopyrrolopyrrole acceptor unit and cyano (CN) groups substituted on the dithiophene ethylene donor unit at different positions. The four small molecules exhibited good thermal stability and solution dispersibility. The bottom gate-bottom contact OFET devices based on these compounds showed excellent *p*-type performances. The relationship between molecular structures and field-effect performances indicated that the alkyl side-chain length and the CN substituted position significantly affected their charge carrier transport properties. The DPP-CN-DTE-1 with side-chain 2-mercaptotetradecyl side-chains and inner-side substituted CN groups exhibited the highest hole mobility of 2.52 $cm^2 V^{-1} s^{-1}$. This work provided a promising approach to develop excellent *p*-type small-molecule semiconductors with high performance, good solution processability and thermal stability for device fabrications.

Introduction

Although *p*-type organic semiconductor materials research has reached an unprecedented height, and more and more high-performance materials have been developed,[1-4] still many improvements and ameliorations should be obtained in the controllability of material structures, purity and so on. Organic conjugated small molecules have important significance for the fabrication of organic field-effect transistors (OFETs) because of their structural certainty, purity and solubility controllability. Molecular engineering by introducing side chains and modifying conjugated skeleton structures has been widely used to develop high-performance *p*-type organic conjugated semiconductors.[5-11] In this work, the length of side chain on the acceptor unit and the relative position of the cyano (CN) groups on the donor unit of the conjugated backbone were respectively adjusted. These adjustments' aim was to obtain *p*-type donor–acceptor (D–A) type conjugated compounds with excellent thermal stability and solution processability. Here, four D–A conjugated organic compounds including diketopyrrolopyrrole (DPP) acceptor units and CN substituted dithiophene ethylene (DTE) donor units were designed and synthesized. The four target conjugated compounds, DPP-CN-DTE-1, DPP-CN-DTE-2, DPP-DTE-CN-1 and DPP-DTE-CN-2, respectively, contain DPP units with different side chains and the DTE units substituted by CN groups in different sites. These four conjugated compounds exhibited good solubility and good thermal stability, providing an important guarantee for the solution processing and performance's annealing optimization of their OFET devices. Based on these D–A type organic small-molecule materials, we fabricated bottom-gate bottom-contact (BGBC) OFET devices, which showed excellent *p*-type charge carrier transport performance. The structure-performance relationship indicated that both the length of the alkyl side chain on the acceptor moiety DPP and the substituting position of CN group on the donor moiety DTE in the conjugated skeleton of the D–A type organic small molecule have different degrees of influence on their charge carrier transport properties. The longer side chain group 2-mercaptotetradecyl and the inside CN substituting positions on DTE are more conducive to the hole transport, thus organic small molecule DPP-CN-DTE-1 exhibited high *p*-type OFET performance with a maximum hole mobility (μ_{hmax}) of 2.52 $cm^2 V^{-1} s^{-1}$.

[a] Beijing National Laboratory for Molecular Sciences, CAS Research/Education Center for Excellence in Molecular Sciences, Institute of Chemistry, Chinese Academy of Sciences, Beijing 100190, P. R. China. E-mail: yugui@iccas.ac.cn
[b] School of Materials Science and Engineering, University of Science and Technology Beijing, Beijing 100083, P. R. China. E-mail: lpwang@mater.ustb.edu.cn
[c] School of Chemical Sciences, University of Chinese Academy of Sciences, Beijing 100049, P. R. China.

Electronic Supplementary Information (ESI) available: [The Device Fabrication and Performance of the OFETs, NMR spectra of the small molecules]. See DOI: 10.1039/x0xx00000x

Experimental

Reagents and reactions

All chemicals were purchased from Acros, Alfa Aesar, Innochem, J&K Scientific, Sigma-Aldrich, etc. The chemicals were used directly if no specified requirement was needed. If

necessary, anhydrous toluene and tetrahydrofuran (THF) were freshly distilled using sodium as scavenger and using benzophenone as indicator according to the standard procedures. P_2O_5 and CaH_2 could be used to treat acetonitrile similarly.

Measurements and characterization of compounds

Proton nuclear magnetic resonance (^{1}H NMR) spectra and carbon nuclear magnetic resonance (^{13}C NMR) spectra of synthetic intermediates were recorded on a Bruker Avance III 400 HD NMR spectrometer. Target compounds were characterized at 100 °C by using a Bruker Avance III 500 WB NMR spectrometer. A 9.4T Solarix FT-ICR mass spectrometer or an APEX II FT-ICR mass spectrometer was used to collect the data of high resolution mass spectroscopy (HRMS) measurements for all the compounds. A PerkinElmer Pyris series TGA8000 thermal analysis system was adopted to carry out the thermaogravimetric analysis (TGA) measurements of target small molecules under N_2 at a heating rate of 10 °C min^{-1}. The ultraviolet-visible-near-infrared (UV–Vis–NIR) absorption spectra of all synthesized small molecules were recorded by using a Hitachi U-3010 spectrophotometer. The electrochemical properties were characterized by using cyclic voltammetry (CV) on a conventional three-electrode type electrochemistry workstation. The HOMO and LUMO energy levels were estimated with the onset of corresponding oxidative and reductive peaks by adopting the equations $E_{HOMO} = -(E_{ox}^{onset} + 4.4)$ eV and $E_{LUMO} = -(E_{re}^{onset} + 4.4)$ eV. A tapping mode Digital Instruments Nanoscope V atomic force microscope (AFM) was adopted to analyze thin film morphologies. The small-molecule thin films were illuminated at a constant incidence angle of 0.2° to obtain their grazing incidence X-ray diffraction (GIXRD) data. The thin film samples used in AFM, GIXRD and FET performance analysis were same.

Synthetic procedure

The synthetic route to conjugated small molecules DPP-CN-DTE-1, DPP-CN-DTE-2, DPP-DTE-CN-1 and DPP-DTE-CN-2 is offered as **Scheme 1**. Intermediate compounds **1–6** were prepared according to the methods reported in literatures. [12-18]

General synthetic and purification procedure of DPP-CN-DTE-1, DPP-CN-DTE-2, DPP-DTE-CN-1 and DPP-DTE-CN-2.

The monomer **2** or **4** (0.60 mmol), bisborate-DPP (**5** or **6**) (0.20 mmol), Na_2CO_3 aqueous solution (2 M, 6 mL), and toluene (15 mL) were added to a 50 mL Schlenk flask. Then $Pd(PPh_3)_4$ (0.06 mmol) and KF (0.4 mmol) were added quickly in one portion after the Schlenk flask was strictly charged with Ar. The mixture was stirred under Ar protection with being heated at 110 °C for 48–96 h. The reaction mixture was poured on a short silica gel pad after being cooled to room temperature (RT) to remove the catalyst and most of salts by using ethyl acetate as an eluent. The filtration was concentrated in vacuo and then purified by silica gel chromatography with eluent of dichloromethane/hexane followed a recrystallization from chloroform/methanol to give the titled compound as a dark green solid.

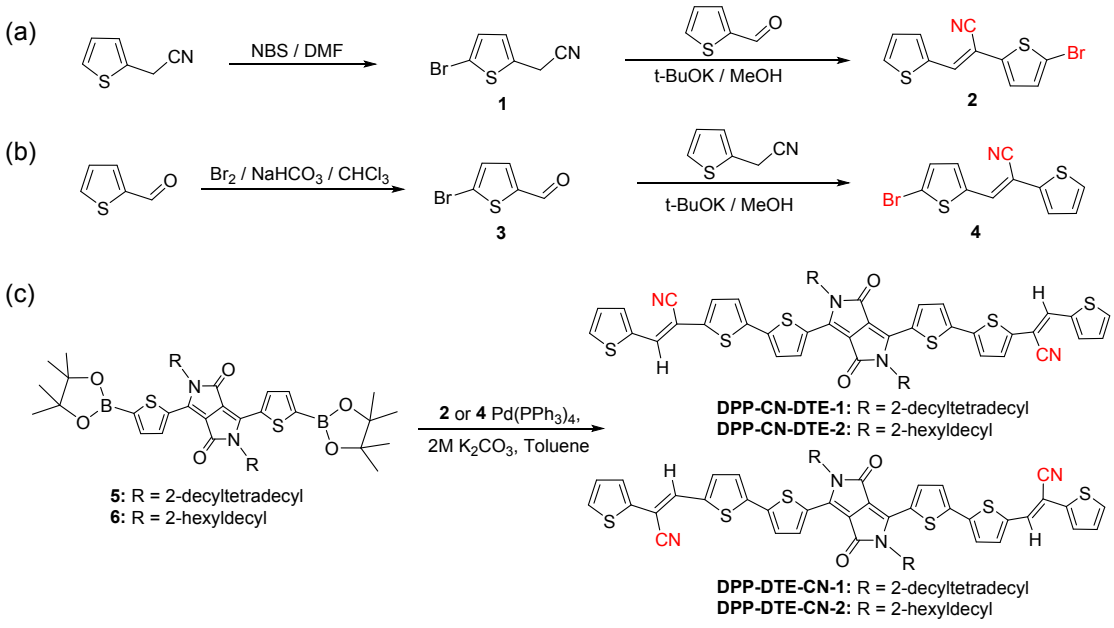

Scheme 1 Synthetic routes of DPP-CN-DTE-n and DPP-DTE-CN-n (n = 1 and 2).

View Article Online
DOI: 10.1039/C9TC03726H

ARTICLE

DPP-CN-DTE-1: (30% yield). ^{1}H NMR (500 MHz, 373K, $CDCl_2CDCl_2$, TMS): δ 8.69 (s, 2H), 7.58 (d, J = 3.7 Hz, 2H), 7.48(d, J = 5.0 Hz, 2H), 7.38 (s, 2H), 7.26(d, J = 4.1 Hz, 2H), 7.21 (d, J = 3.9 Hz, 2H), 7.18 (s, 2H), 7.08 (t, J = 5.0 Hz, 2H), 3.95 (d, J = 10.0 Hz, 4H), 1.91 (s, 2H), 1.27–1.16 (br, 80H), 0.80–0.77 (dt, J = 5.0 Hz, J = 5.0 Hz, 12H). ^{13}C-NMR (126 MHz, 373K, $CDCl_2CDCl_2$, TMS): δ 161.63, 141.39, 139.45, 137.63, 136.78, 136.08, 132.26, 132.23, 130.52, 129.37, 128.20, 127.87, 125.96, 125.48, 116.35, 109.33, 103.00, 46.73, 38.14, 31.83, 30.00, 29.62, 29.59, 29.51, 29.24, 26.57, 22.56, 13.93. HRMS (MALDI): calcd. for $C_{84}H_{115}N_4O_2S_6$ $[M+H]^+$ (1403.7339); found: 1403.7327.

DPP-CN-DTE-2: (25% yield). ^{1}H NMR (500 MHz, 373K, $C_6Cl_2D_4$, TMS): δ 8.84 (d, J = 5.0 Hz, 2H), 7.30 (s, 2H), 7.138.84 (d, J = 5.0 Hz, 2H), 7.10 (s, 2H), 7.01 (s, 2H), 6.99 (s, 2H), 6.92 (s, 4H), 3.95 (d, J = 10.0 Hz, 4H), 1.94 (s, 2H), 1.27–1.06 (br, 48H), 0.64 (s, 12H). ^{13}C-NMR (126 MHz, 373K, $C_6Cl_2D_4$, TMS): δ 161.27, 141.12, 139.38, 139.02, 137.51, 136.65, 136.06, 131.83, 131.50, 129.89, 129.38, 127.70, 127.41, 125.49, 125.11, 115.90, 109.30, 102.88, 46.50, 38.27, 31.72, 31.72, 31.64, 29.99, 29.58, 29.42, 29.14, 26.46, 26.40, 22.45, 22.43, 13.68. HRMS (MALDI): calcd. for $C_{68}H_{83}N_4O_2S_6$ $[M+H]^+$ (1179.4835); found: 1179.4839.

DPP-DTE-CN-1: (28% yield). ^{1}H NMR (500 MHz, 373K, $C_6Cl_2D_4$, TMS): δ 8.84 (d, J = 5.0 Hz, 2H), 7.18 (s, 2H), 7.03 (d, J = 5.0 Hz, 6H), 6.98 (d, J = 5.0 Hz, 2H), 6.91 (d, J = 5.0 Hz, 2H), 6.67 (d, J = 5.0 Hz, 2H), 3.95 (d, J = 10.0 Hz, 4H), 1.94 (s, 2H), 1.28–1.03 (br, 80H), 0.65 (t, J = 5.0 Hz, 12H). ^{13}C-NMR (126 MHz, 373K, $C_6Cl_2D_4$, TMS): δ 161.25, 140.99, 139.96, 139.02, 138.81, 137.90, 136.13, 132.68, 130.29, 129.99, 127.86, 127.01, 126.05, 125.63, 125.23, 116.33, 109.49, 103.83, 46.53, 38.30, 31.74, 30.02, 29.58, 29.51, 29.17, 26.48, 22.45, 13.68. HRMS (MALDI): calcd. for $C_{84}H_{114}N_4NaO_2S_6$ $[M+Na]^+$ (1425.7158); found: 1425.7162.

DPP-DTE-CN-2: (20% yield). ^{1}H NMR (500 MHz, 373K, $CDCl_2CDCl_2$, TMS): δ 8.69 (d, J = 3.2 Hz, 2H), 7.48 (d, J = 3.6 Hz, 2H), 7.34 (d, J = 3.8 Hz, 2H), 7.31 (s, 2H), 7.27 (d, J = 3.0 Hz, 2H), 7.25 (d, J = 4.2 Hz, 4H), 6.99 (d, J = 4.0 Hz, 2H), 3.93 (d, J = 7.4 Hz, 4H), 1.88 (s, 2H), 1.36–1.06 (br, 48H), 0.77 (t, J = 5.0 Hz, 12H). ^{13}C NMR (126 MHz, 373K, $CDCl_2CDCl_2$, TMS): δ 160.68, 140.32, 139.31, 138.54, 137.94, 137.14, 135.19, 132.10, 130.11, 129.02, 127.42, 126.25, 125.64, 125.18, 124.86, 115.82, 108.60, 103.04, 45.81, 37.22, 30.87, 30.76, 29.05, 28.69, 28.66, 28.50, 28.25, 25.61, 25.57, 21.62, 21.58, 13.00. HRMS (MALDI): calcd. for $C_{68}H_{82}N_4NaO_2S_6$ $[M+Na]^+$ (1201.4654); found: 1201.4646.

Results and discussion

Synthesis and thermal properties

In order to obtain CN-substituted DTE donor units, key intermediates **2** and **4**, we used the Knoevenagel condensation reaction method reported in the literature,[19] under the action of a strong base potassium *t*-butoxide. For the preparation of the necessary intermediates **1** and **3**, we respectively adopted the method of NBS radical reaction[20] and the method of liquid bromine bromination under alkaline conditions.[21] The DPP acceptor units (intermediate compounds **5** and **6**) were prepared by the method of extracting hydrogen with lithium diisopropylamide (LDA) according to the literatures.[12-18] Finally, CN-substituted DTE donor units **2** or **4** were coupled with DPP receptor units **5** or **6** using the Suzuki coupling method with catalyst $Pd(PPh_3)_4$ to prepare four target conjugated compounds DPP-CN-DTE-1, DPP-CN-DTE- 2, DPP-DTE-CN-1 and DPP-DTE-CN-2, respectively. The synthetic route of the target compounds and intermediates is shown in **Scheme 1.** The final products DPP-CN-DTE-1, DPP-CN-DTE-2, DPP-DTE-CN-1 and DPP-DTE-CN-2 were structurally confirmed by the NMR spectra and HRMS data. At the same time, in order to ensure the feasibility of annealing in subsequent OFET device processing to optimize carrier transport performance, the good thermal stability of the organic compounds is necessary. It is considered that thermogravimetric analysis (TGA) can usually be used to detect the thermal properties of organic semiconductors.[22] TGA tests of these conjugated compounds were performed with results shown in **Fig. S1** and the corresponding data are listed in **Table 1**. The four conjugated compounds DPP-CN-DTE-1, DPP-CN-DTE-2, DPP-DTE-CN-1 and DPP-DTE-CN-2 showed their 5% weight loss at 404.7, 396.0, 402.0 and 396.3 °C, respectively. These temperature data indicated that these compounds showed good thermal stability. It provides good stability guarantee for the optimization of annealing in the preparation of their OFET devices.

Optical properties

We measured the photophysical properties of four DPP-DTE-based conjugated compounds DPP-CN-DTE-1, DPP-CN-DTE-2, DPP-DTE-CN-1 and DPP-DTE-CN-2 by using UV-Vis-NIR absorption spectroscopy. The UV-Vis-NIR absorption spectra of the four compounds in a chloroform solution (concentration 10^{-5} M) and on a quartz plate are shown in **Figs. 1 and S2**. In chloroform solution, the maximum absorption wavelengths of DPP-CN-DTE-1, DPP-CN-DTE-2, DPP-DTE-CN-1 and DPP-DTE-CN-2 were 624, 632, 632 and 623 nm, respectively, with almost no significant difference. In the thin films, the maximum absorption wavelengths of DPP-CN-DTE-1, DPP-CN-DTE-2, DPP-DTE-CN-1 and DPP-DTE-CN-2 were 760, 753, 762 and 752 nm, respectively, also without significant difference. However, by comparing the absorption in solution and thin film, we found two differences. The one difference was that the corresponding absorption peak of the maximum absorption wavelength of each material in solution was found close to the Gaussian distribution while those in films

exhibited obvious shoulder peaks. The maximum absorption wavelength of the thin films showed red shifted above 120 nm (121–136 nm) compared to those in the respective solution. It can be seen that the aggregation of the four materials in the film is much higher than that in the corresponding solution. It can be also reflected from the side angle that there was a high degree of dispersion for this series of materials in the chloroform solution. And there is almost no pre-aggregation phenomenon for these four materials in solution, which should be beneficial for the processing of corresponding OFET devices by solution method. The peak shapes of the absorption peaks at the maximum absorption wavelength of the four materials are almost identical for each both in the solution and film state. It is reflecting to some extent that the dispersion degree in chloroform solution and the aggregation degree in film state are almost the same for each of the four materials.

In addition, the onset of the UV-Vis-NIR absorption spectrum (λ_{onset}) of the films was used to calculate the optical band gap E_g(opt) based on the formula E_g(opt) = 1240/λ_{onset}. The absorption onsets of DPP-CN-DTE-1, DPP-CN-DTE-2, DPP-DTE-CN-1 and DPP-DTE-CN-2 are 842, 865, 878 and 872 nm,

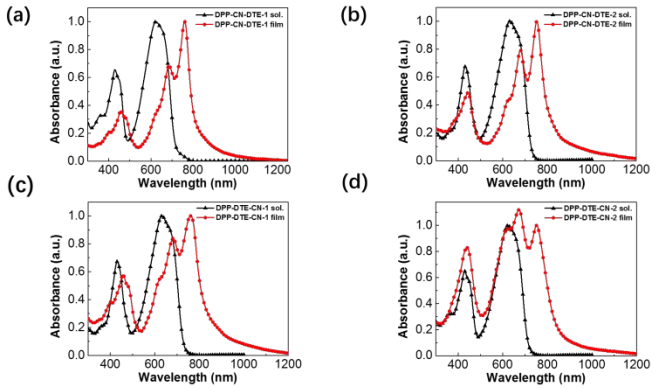

Fig. 1 UV-Vis-NIR absorption spectra of the conjugated compounds (a) DPP-CN-DTE-1, (b) DPP-CN-DTE-2, (c) DPP-DTE-CN-1 and (d) DPP-DTE-CN-2 in chloroform solutions and thin films.

Table 1 Thermal, optical and electrochemical properties of small molecules based on DPP-DTE

Compd	T_d[a] (°C)	λ_{max}[b] (solution)(nm)	λ_{max}[b] (film)(nm)	E_g(opt)[c] (eV)	E_{HOMO} (eV)	E_{LUMO} (eV)
DPP-CN-DTE-1	404.7	624	760	1.47	-5.18	-3.65
DPP-CN-DTE-2	396.0	632	753	1.43	-5.25	-3.72
DPP-DTE-CN-1	402.0	632	762	1.41	-4.86	-3.70
DPP-DTE-CN-2	396.3	623	752	1.42	-4.85	-3.71

[a] Temperature at 5% weight loss. [b] Maximum absorption wavelengths in chloroform solution and film state. [c] Calculated according to the wavelength at the peak onset in the UV-Vis-NIR absorption spectra in the film state.

respectively, which were brought into the above formula to obtain the optical band gap of the compounds. Their optical band gaps of 1.47, 1.43, 1.4, and 1.42 eV (**Table 1**) from DPP-CN-DTE-1, DPP-CN-DTE-2 to DPP-DTE-CN-1, and DPP-DTE-CN-2 show a gradual narrowing trend. The trend of band gap narrowing from DPP-CN-DTE-1 to DPP-CN-DTE-2 is slightly more pronounced, while DPP-DTE-CN-1 and DPP-DTE-CN-2 showed almost no significant difference. This phenomenon can reflect a fact that for small molecules, when the CN group is close to the DPP acceptor unit, the length of the alkyl side chain on the acceptor unit generated a relatively significant effect impacting on the optical band gap. The above results indicated that the aggregation state's difference of these conjugated compounds in the solution and film states is significant. But on the conjugated backbone, neither the CN substitution position of the donor unit nor the different length of the alkyl side chain on the acceptor unit shows significant effect impacting on the absorption spectra.

Electrochemical Properties

We used cyclic voltammetry (CV) to study the electrochemical performance of the four conjugated compounds based on DPP-DTE. In the CV test, silver/silver chloride (Ag/AgCl) was used as a reference electrode, trace ferrocene as an internal standard, and a Pt electrode coated with a thin film of the conjugated compound as a working electrode. All measurements were carried out at room temperature under a nitrogen atmosphere. The HOMO and LUMO energy levels of the conjugated compounds were estimated by using the equations $E_{HOMO} = -(E_{ox}^{onset} + 4.4)$ eV and $E_{LUMO} = -(E_{re}^{onset} + 4.4)$ eV at the starting point of the respective oxidation peaks and reduction peaks.[23] The initial oxidation/reduction potentials of DPP-CN-DTE-1, DPP-CN-DTE-2, DPP-DTE-CN-1, and DPP-DTE-CN-2 are located at 0.78/-0.75 eV, 0.85/-0.68 eV, 0.46/−0.70 eV and 0.45/−0.69 eV, respectively (**Fig. 2**). As shown in **Table 1**, based on these initial potential values and calculated according to the above equations, the HOMO/LUMO energy levels of the compounds DPP-CN-DTE-1, DPP-CN-DTE-2, DPP-DTE-CN-1 and DPP-DTE-CN-2 were –5.18/–3.65, –5.25/–3.72, –4.86/–3.70 and –4.85/–3.71 eV, respectively. These observations indicate that the position of the CN substitution of the conjugated backbone has a

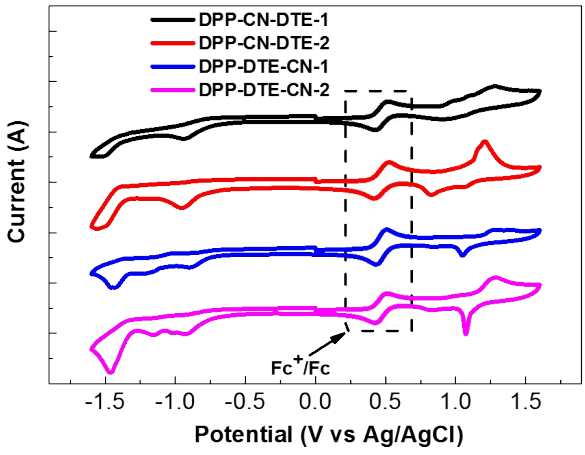

Fig. 2 Cyclic voltammetry curves of the thin films for the DPP-DTE-based compounds in an acetonitrile solution containing 0.1 M electrolyte n-Bu_4NPF_6 and trace ferrocene as internal standard.

significant effect on their HOMO energy levels, while the alkyl side chain has no significant effect. In addition, the differences between the electrochemical band gaps and the optical band gaps of these four small-molecule compounds are 0.06–0.28 eV, which is within the acceptable experimental error range according to the literature.[24]

Theoretical calculations

To further understand the frontier molecular orbital features the molecular geometries, we replaced the alkyl side chain with methyl group to simply the two small molecules DPP-DTE-CN-1 and DPP-CN-DTE-1 before theoretically calculated them using Guassian 09 software at the density functional theory (DFT)/B3LYP/6-31G (d) level. The theoretical calculation results (**Fig. S3**) show that both the molecules possess very good planarity, the introduction of the CN unit does not cause the distortion of the molecular backbone, and their HOMO and LUMO are all delocalized throughout the molecular backbone. The difference in the position of the CN unit does not cause a significant difference in the HOMO and LUMO energy levels of the two molecules. It is speculated that the significant difference of their HOMO energy levels obtained from the above CV detections maybe due to the influence of the inter-molecular arrangement and crystallization caused by the interaction of the alkyl chain and the inner CN group.

Charge carrier transport performance.

In order to study the field-effect characteristics of the four DPP-DTE-based compounds, the OFET devices with the BGBC configurations were fabricated. We annealed the thin films of the DPP-DTE-based compounds DPP-CN-DTE-1, DPP-CN-DTE-2, DPP-DTE-CN-1 and DPP-DTE-CN-2 at their own optimal annealing-temperatures of 140, 180, 100 and 100 °C, respectively. All OFET devices based on the compounds DPP-CN-DTE-1, DPP-CN-DTE-2, DPP-DTE-CN-1 and DPP-DTE-CN-2 exhibited *p*-type field-effect properties under air conditions. Typical transfer and output curves for OFET devices based on the four compounds are shown in **Fig. 3**, and the corresponding parameters are collected in **Table 2**. The listed saturation mobilities were obtained from the transfer curves of the OFET devices. Among the four compounds, DPP-CN-DTE-1 showed much higher hole mobility than those of the other three materials. The highest hole mobility of DPP-CN-DTE-1 reached 2.52 $cm^2\ V^{-1}\ s^{-1}$, which was two orders of magnitude higher compared with the other three compounds. The highest hole mobility of the materials DPP-CN-DTE-2, DPP-DTE-CN-1 and DPP-DTE-CN-2 were 1.92×10^{-2}, 2.30×10^{-2} and 2.17×10^{-2} $cm^2\ V^{-1}\ s^{-1}$, respectively. The above results indicated that the CN groups on the inner side with a larger alkyl side chain substituted on the DPP were beneficial for greatly increasing the carrier transport properties and obtaining higher hole mobility.

Characterization of thin film microstructure

To further understand the relationship between the field-effect properties of DPP-DTE-based compounds and their molecular structures, the intermolecular stacking and surface topography of their thin films were studied by means of 2D-GIXRD and AFM experiments. **Figure 4** shows the 2D-GIXRD patterns of the thin films for the four compounds DPP-CN-DTE-1, DPP-CN-DTE-2, DPP-DTE-CN-1 and DPP-DTE-CN-2 before and after annealing at their own optimal annealing-temperatures 140, 180, 100 and 100 °C, respectively. We found through the

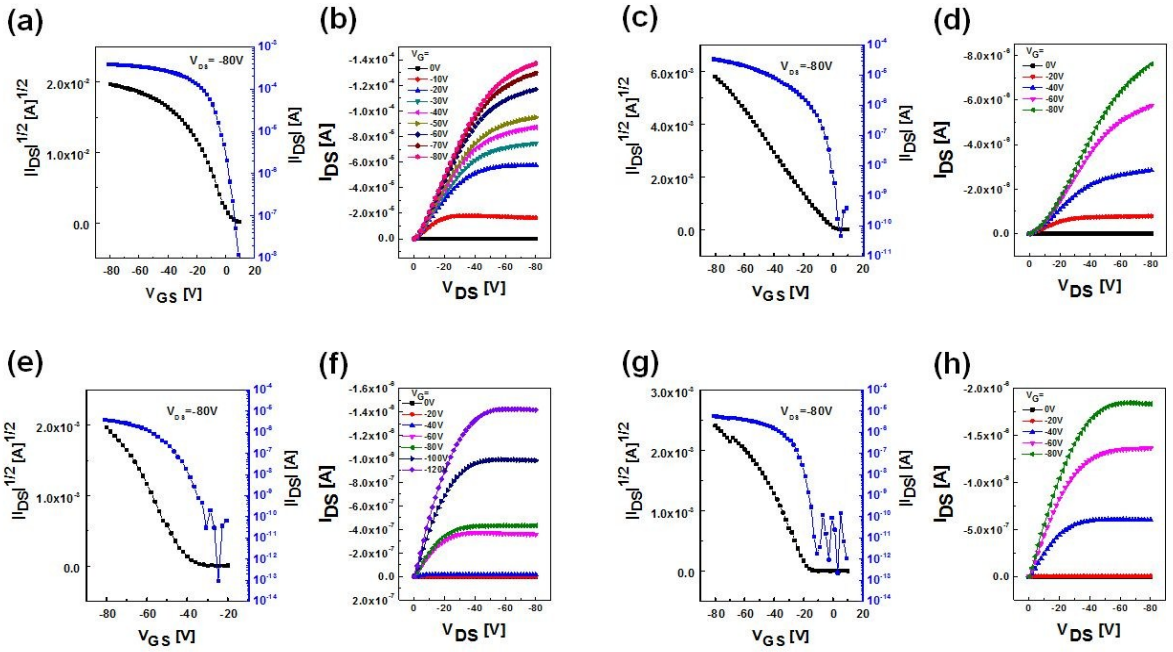

Fig. 3 Transfer and output curves of the OFET devices based on the compounds (a,b) DPP-CN-DTE-1, (c,d) DPP-CN-DTE-2, (e,f) DPP-DTE-CN-1 and (g,h) DPP-DTE-CN-2 after annealing at 140, 180, 100 and 100 °C, respectively.

View Article Online
DOI: 10.1039/C9TC03726H

Table 2 The performances of OFET devices with BGBC configurations and relevant crystallographic parameters of thin films for the DPP-DTE-based compounds

Compd	μ_{hmax} (rt/annealed) ($cm^2\ V^{-1}\ s^{-1}$)	I_{ON}/I_{OFF}	V_{th} (V)	d–d^a(Å)	π–π^a (Å)
DPP-CN-DTE-1	0.96 / 2.52	10^4–10^5	2.32	17.4	3.48
DPP-CN-DTE-2	8.26×10^{-3} / 1.92×10^{-2}	10^5–10^6	–4.57	15.0	3.50
DPP-DTE-CN-1	1.08×10^{-2} / 2.30×10^{-2}	10^7–10^8	–42.55	24.7	3.98
DPP-DTE-CN-2	1.04×10^{-2} / 2.17×10^{-2}	10^7–10^8	–18.30	17.7	3.56

[a] The stacking distances calculated from the annealed films.

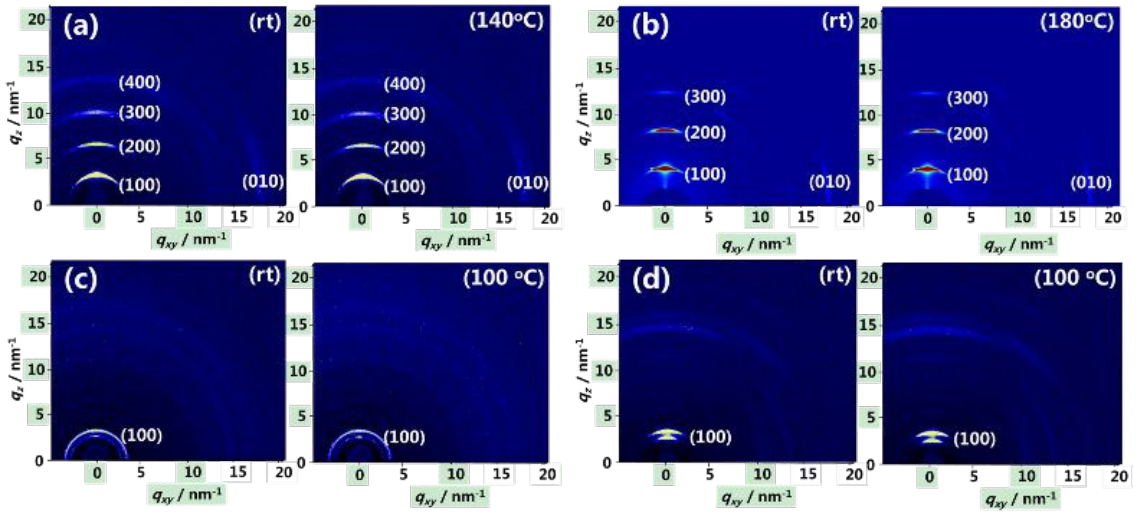

Fig. 4 GIXRD patterns of the (a) DPP-CN-DTE-1, (b) DPP-CN-DTE-2, (c) DPP-DTE-CN-1 and (d) DPP-DTE-CN-2 thin films before and after annealing at 140, 180, 100 and 100 °C, respectively.

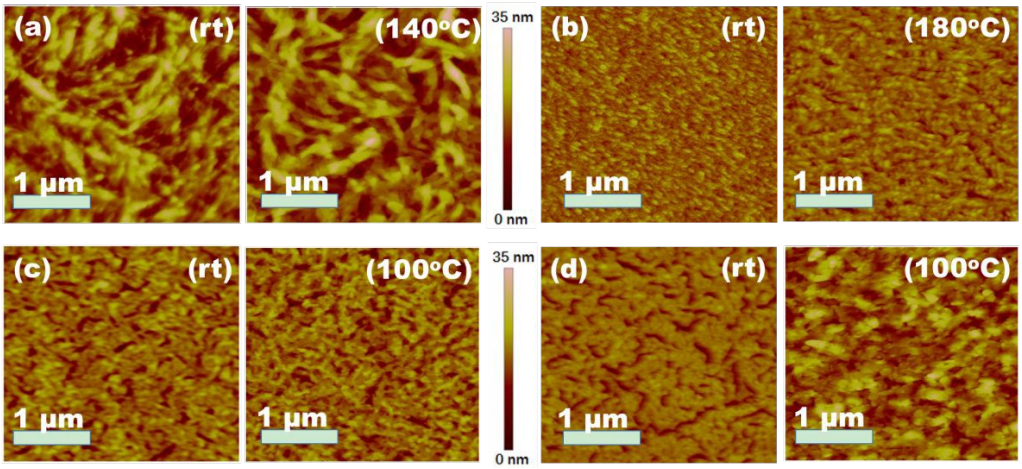

Fig. 5 AFM height maps of the (a) DPP-CN-DTE-1, (b) DPP-CN-DTE-2, (c) DPP-DTE-CN-1 and (d) DPP-DTE-CN-2 thin films before and after annealing at 140, 180, 100 and 100 °C, respectively.

corresponding processing and analysis of **Fig. 4** that d–d separation distance values of 17.4, 15.0, 24.7 and 17.7 Å were corresponding to the out-of-plane (q_z)-oriented (100) Bragg peaks of the DPP-CN-DTE-1, DPP-CN-DTE-2, DPP-DTE-CN-1 and DPP-DTE-CN-2 thin films, respectively. In the in-plane (q_{xy}) orientation, the four thin films had distinct (010) Bragg in-

plane peaks, in which DPP-CN-DTE-1 and DPP-CN-DTE-2 were particularly significant. The corresponding π–π stacking distances of DPP-CN-DTE-1, DPP-CN-DTE-2, DPP-DTE-CN-1 and DPP-DTE-CN-2 were 3.48, 3.50, 3.98, and 3.56 Å, respectively. All of the above related parameters can be found in **Table 2**. According to the (010) Bragg peaks in the in-plane (q_{xy}) and out-of-plane (q_z) directions provided by the 2D-GIXRD spectra, we can infer that among the four compounds, both DPP-CN-DTE-1 and DPP-CN-DTE-2 tend to adopt edge-on packing mode, while the DPP-DTE-CN-1 and DPP-DTE-CN-2 are amorphous in Fig. 4. In this mode, the thin films of DPP-CN-DTE-1 and DPP-CN-DTE-2 with the electron-absorbing CN groups on the donor unit DTE and near to the acceptor unit DPP (inner-side) showed a more obvious edge-on-based molecular packing pattern. Interestingly, the DPP-CN-DTE-1 thin film showed the strongest (h00) diffraction peaks from (100) up to (400) (**Fig. 4a**). The DPP-CN-DTE-2 thin film exhibited strong (h00) diffraction peaks from (100) up to (300) (**Fig. 4b**). Meanwhile, the thin films of DPP-DTE-CN-1 and DPP-DTE-CN-2 with CN groups substituted on outer-side only showed diffraction peaks of (100) (**Fig. 4c** and **4d**). This phenomenon indicated that among these four DPP-DTE-based small-molecule compounds, DPP-CN-DTE-1 and DPP-CN-DTE-2 with the CN groups substituted on the inner-side exhibited better crystallinity and more ordered layer-structure than those of DPP-DTE-CN-1 and DPP-DTE-CN-2 with CN substituted on the outer-side. In addition, from **Fig. 4**, we also observed that both the length of the alkyl side chain on the DPP unit and the annealing treatment of the films exhibited no obvious influence on the ordering of the molecular layer-structure.

For the surface morphology of thin films of the four DPP-DTE-based compounds, we used the Tapping mode AFM for detection. The height profiles of the DPP-CN-DTE-1, DPP-CN-DTE-2, DPP-DTE-CN-1 and DPP-DTE-CN-2 thin films before and after annealing at their own optimal annealing-temperatures 140, 180, 100 and 100 °C, respectively, are shown in **Fig. 5**. The temperatures before and in annealing were room temperature (rt) and the optimum annealing ones, respectively. The morphologies of the four thin films were improved to some extent after annealing. The morphology of the DPP-CN-DTE-1 film both before and after annealing showed obvious fish bone combined with the mesh shape. This kind of surface morphology of the film is generally favourable for the charge carrier transport, which can prove the high mobility of the compound DPP-CN-DTE-1 from a certain angle. The films of the other three compounds DPP-CN-DTE-2, DPP-DTE-CN-1 and DPP-DTE-CN-2 showed a granular morphology before and after annealing. This granular morphology reflected the arrangement continuity among the molecules of the material was relatively poor, and even there were relatively obvious grain boundaries, which were obviously not conducive to charge carrier transport. The apparent difference in morphology of the above-mentioned four thin films may lead to the difference in their charge carrier mobility. It can be reflected from the side for the inevitability that the compound DPP-CN-DTE-1 exhibited a higher hole-mobility than DPP-CN-DTE-2, DPP-DTE-CN-1 and DPP-DTE-CN-2 did.

These 2D-GIXRD and AFM results of the four DPP-DTE-based compounds were combined with charge carrier transport mobilities. We found that the CN substitution position on the DTE donor unit had a great influence on the compound's electronic structure, the film's surface morphology, molecular packing mode and carrier mobility. In other words, the position of the CN played an important role in regulating the electronic structure of the molecule, the accumulation between the conjugated backbones, and the intermolecular interaction, and thus affecting the microstructure of the thin film and carrier transport performance.[25-28] The CN groups on the inner-side of the molecule backbone was beneficial to lower the HOMO energy levels, and their corresponding thin films were advantageous for adopting a more orderly layered stacking pattern. Under the combination of the inner-side substituted CN groups and the larger 2-mercaptotetradecyl group on the DPP unit, the DPP-CN-DTE-1 was more favourable to exhibit a continuous film morphology and thus was more conducive for charge carrier transport to achieve higher *p*-type field-effect performance.

Conclusions

Four DPP-DTE-based D–A type conjugated small-molecule compounds DPP-CN-DTE-1, DPP-CN-DTE-2, DPP-DTE-CN-1 and DPP-DTE-CN-2 were designed and synthesized by tuning alkyl side chain size and electron-withdrawing group CN substitution position. Their thermal properties, optical absorption spectra, electrochemical properties, carrier transport properties, microscopic arrangement and surface morphology of the films were systematically studied. The compounds show good thermal stabilities and solution dispersibility, which provided guarantees for the solution processing and annealing optimization of their OFET devices. The substituted position of CN had a great influence on the electronic structure, film surface morphology, molecular packing mode and carrier mobility of these compounds. The CN on the inner-side was favorable for lowering the HOMO energy levels and adopting orderly layered packing mode in thin film. The structure-performance relationship indicated that the alkyl side-chain length and the CN substituted position significantly affected the carrier transport properties. Combined with inner-side substituted CN and longer side-chain 2-mercaptotetradecyl, the DPP-CN-DTE-1 exhibited a more continuous film morphology, which was more conducive for charge carrier transport to obtain higher *p*-type OFET performance than those of other three compounds. Among these four compounds, DPP-CN-DTE-1 showed the highest OFET performance with its maximum hole-mobility of 2.52 $cm^2 V^{-1} s^{-1}$. The above results provided a promising approach to develop excellent small-molecular OFET materials with high hole-mobility, good solution processability and good thermal stability.

Conflicts of interest

There are no conflicts to declare.

Acknowledgements

This work was supported under the financial support from the National Key Research and Development Program of China (2017YFA0204703 and 2016YFB0401100) and the National Natural Science Foundation of China (51773016, 21673258, and 21774134). The scientists from 1W1A station of Beijing Synchrotron Radiation Facility (BSRF) and the BL14B1 Station of Shanghai Synchrotron Radiation Facility (SSRF) gave much assistance during the GIXRD tests for this work. The authors sincerely thank them all.

Notes and references

1. D. X. Long, E. Y. Choi and Y. Y. Noh, *ACS Appl. Mater. Interfaces*, 2017, **9** , 24763-24770.
2. M. Wang, M. J. Ford, A. T. Lill, H. Phan, T. Q. Nguyen and G. C. Bazan, *Adv. Mater.*, 2017, **29**, 1603830.
3. B. Fu, J. Baltazar, A. R. Sankar, P. H. Chu, S. Zhang, D. M. Collard and E. Reichmanis, *Adv. Funct. Mater.*, 2014, **24**, 3734-3744.
4. J. Y. Back, H. Yu, I. Song, I. Kang, H. Ahn, T. J. Shin, S. K. Kwon, J. H. Oh and Y. H. Kim, *Chem. Mater.*, 2015, **27**, 1732-1739.
5. S. Ghosh, R. Raveendran, A. Saeki, S. Seki, M. A. Namboothiry and A. Ajayaghosh, *ACS Appl. Mater. Interfaces*, 2019, **11**, 1088-1095.
6. T. He, P. Leowanawat, C. Burschka, V. Stepanenko, M. Stolte and F. Wurthner, *Adv. Mater.*, 2018, 1804032.
7. B. Lim, H. Sun and Y. Y. Noh, *Dyes Pigments*, 2017, **142**, 17-23.
8. B. Lim, H. Sun, J. Lee and Y. Y. Noh, *Sci. Report.*, 2017, **7**, 164.
9. G. Zhang, Y. Zhao, B. Kang, S. Park, J. Ruan, H. Lu, L. Qiu, Y. Ding and K. Cho, *Chem. Mater.*, 2019, **31**, 2027-2035.
10. K. Hyodo, S. Nishinaga, Y. Sawanaka, T. Ishida, H. Mori and Y. Nishihara, *J. Org. Chem.*, 2019, **84**, 698-709.
11. T. Delouche, A. Mocanu, T. Roisnel, R. Szucs, E. Jacques, Z. Benko, L. Nyulaszi, P. A. Bouit and M. Hissler, *Org. Lett.*, 2019, **21**, 802-806.
12. K. Shi, W. Zhang, C. Wei, Z. Lin, X. Liu and G. Yu, *J. Polym. Sci., Part A: Polym. Chem.*, 2018, **56**, 1012-1019.
13. G. Conboy, R. G. D. Taylor, N. J. Findlay, A. L. Kanibolotsky, A. R. Inigo, S. S. Ghosh, B. Ebenhoch, L. K. Jagadamma, G. K. V. V. Thalluri, M. T. Sajjad, I. D. W. Samuel and P. J. Skabara, *J. Mater. Chem. C*, 2017, **5**, 11927-11936.
14. W. Zhang, Z. Mao, N. Zheng, J. Zou, L. Wang, C. Wei, J. Huang, D. Gao and G. Yu, *J. Mater. Chem. C*, 2016, **4**, 9266-9275.
15. H. Burckstummer, A. Weissenstein, D. Bialas and F. Wurthner, *J. Org. Chem.*, 2011**, 76**, 2426-2432.
16. J. Lee, S. Cho, J. H. Seo, P. Anant, J. Jacob and C. Yang, *J. Mater. Chem.*, 2012, **22**, 1504-1510.
17. D. Cortizo-Lacalle, S. Arumugam, S. E. T. Elmasly, A. L. Kanibolotsky, N. J. Findlay, A. R. Inigo and P. J. Skabara, *J. Mater. Chem.,* 2012, **22**, 11310-11315.
18. J. Lee, A. R. Han, J. Hong, J. H. Seo, J. H. Oh and C. Yang, *Adv. Funct. Mater.,* 2012, **22**, 4128-4138.
19. H. J. Yun, S. J. Kang, Y. Xu, S. O. Kim, Y. H. Kim, Y. Y. Noh and S. K. Kwon, *Adv. Mater.*, 2014, **26**, 7300-7307.
20. N. S. Cho, D. H. Hwang, B. J. Jung, E. Lim, J. Lee and H. K. Shim, *Macromolecules*, 2004, **37**, 5265-5273.
21. F. Yang, X. L. Xu, Y. H. Gong, W. W. Qiu, Z. R. Sun, J. W. Zhou, P. Audebert and J. Tang, *Tetrahedron*, 2007, **63**, 9188-9194.
22. Y. Li, S. P. Singh and P. Sonar, *Adv. Mater.,* 2010, **22**, 4862-4866.
23. Y. Cui, X. Zhang and S. A. Jenekhe, *Macromolecules*, 1999, **32**, 3824-3826.
24. D. Gao, Z. Chen, Z. Mao, J. Huang, W. Zhang, D. Li and G. Yu, *RSC Adv.,* 2016, **6**, 78008-78016.
25. J. Mei, D. H. Kim, A. L. Ayzner, M. F. Toney and Z. Bao, *J. Am. Chem. Soc.*, 2011**, 133**, 20130-20133.
26. J. Lee, A. R. Han, J. Kim, Y. Kim, J. H. Oh and C. Yang, *J. Am. Chem. Soc.,* 2012, **134**, 20713-20721.
27. J. Yao, C. Yu, Z. Liu, H. Luo, Y. Yang, G. Zhang and D. Zhang, *J. Am. Chem. Soc.*, 2016, **138**, 173-185.
28. W. Zhang, Z. Chen, Z. Mao, D. Gao, C. Wei, Z. Lin, J. Huang, L. Wang and G. Yu, *Dyes Pigments*, 2018, **149**, 149-157.

View Article Online
DOI: 10.1039/C9TC03726H

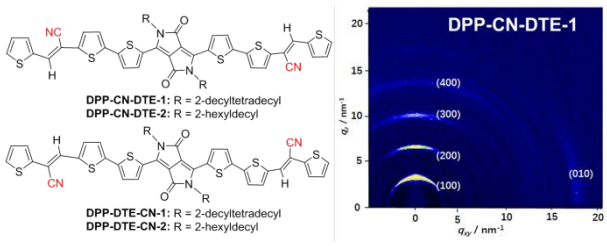

Small-molecule compounds based on diketopyrrolopyrrole and cyano substituted dithiophene-ethylene were synthesized and their properties were systematically studied.